Springer

KSME

Journal of Mechanical Science and Technology 25 (10) (2011) 2467~2474
www.springerlink.com/content/1738-494x
DOI 10.1007/s12206-011-0734-z

# Robust controller for an autonomous vehicle with look-ahead and look-down information †

Ju Yong Choi*

*Department of Mechatronics Engineering, Kyungsung University, Busan, 608-736, Korea*

(Manuscript Received January 13, 2010; Revised April 4, 2011; Accepted July 11, 2011)

**Abstract**

For the lateral control of an autonomous vehicle, this paper proposes a linear-matrix-inequality (LMI)-based $H_\infty$ control algorithm that utilizes the feedback of the lateral offset and target yaw angle at the preview point, which is effective for the fusion of look-ahead and look-down sensors. To verify the performance of this controller, lane change and circular lane tracking simulations are carried out in multi body dynamics. Against the uniformly random noises in position and yaw angle and the constant modeling uncertainties in mass and cornering stiffness, the robustness of the proposed algorithm is compared with the cubic curve method and the heading angle method at the look-ahead target lane.

*Keywords*: Autonomous vehicle; Lateral control; LMI-based $H_\infty$ control; Look-ahead sensing; Multi body dynamics

## 1. Introduction

Autonomous vehicle systems have two basic control tasks: longitudinal control and lateral control. Longitudinal control involves joining a fleet, splitting from it, and regulating the speed to maintain proper spacing between vehicles. Lateral control, or lane-keeping, involves autonomously guiding the vehicle to reference trajectories. By using the relative lateral offset and heading of the vehicle, various lateral control algorithms have previously been proposed [1-3], and Ref. [4]. A robust lateral controller was designed against the variations in velocity, mass, and road-tire contact [5]. These intelligent vehicle systems have been applied to buses and transport vehicles [6] on routine roadways. In the research by Makela and Numers [7], an autonomously guided outdoor vehicle used to transport heavy steel slabs in a steel plant area was developed.

In the case of references on a roadway, the reference and sensing systems are classified into two categories [1, 2]: look-down systems and look-ahead systems. In the look-down method, inductive cables were used to mark the reference lane. In the PATH project [1, 8], permanent magnets were used to mark the reference roadways; four magnetic sensors detect the markers when the vehicle passes by them. In the look-ahead method, machine vision [2], radar, or ultrasonic sensor [7] was used. Machine vision systems have passive reference or passive sensing systems [9]. The alarm system of traffic line separation [10] and the unmanned traveling equipment utilized the vision systems. Unlike the case of the look-down method, it is easy to mark the reference lane, but the detected information is heavily affected by weather conditions. The references are not on the roadway; instead, they are on an electronic road map in the global positioning system (GPS) and the inertial navigation system (INS).

In conventional lateral control that utilize look-ahead information of the lane, Tsugawa [2] designed a lateral controller based on the non slip model. Lee [12] introduced the lateral controller to minimize the target heading angle about target points. In this study, linear-matrix-inequality (LMI)-based $H_\infty$control through the feedback of the target heading angle is used to design a lateral controller that is robust against high-frequency sensor noise and modeling uncertainty. Furthermore, to reduce tracking error, the lateral controller is modified by the feedback of the target yaw angle at the preview point and the lateral offset at the vehicle center of gravity (CG).

The remainder of this paper is organized as follows. First, Section 2 describes vehicle models. The lateral model is verified by a J-turn test and is compared with the multi body dynamics of a vehicle and actual vehicle responses. In Section 3, a LMI based $H_\infty$controller for lateral control is designed using look-ahead and look-down information. The robustness is simulated in the multi body dynamics in Section 4. Finally, Section 5 summarizes the results presented in this paper.

† This paper was recommended for publication in revised form by Associate Editor Kyongsu Yi
* Corresponding author. Tel.: +82 51 663 4695, Fax.: +82 51 624 5980
E-mail address: jychoi@ks.ac.kr

## 2. Vehicle modeling and verification

In this section, a two degrees of freedom (DOF) model (in other words, a single-track model) for a controller design and a 79 degrees of freedom multi body dynamic model for simulations are described and verified by a J-turn test. The result of the J-turn test is compared with actual vehicle's responses.

### *2.1 Two degrees of freedom vehicle model*

Yaw rate and lateral acceleration as lateral performance are calculated by the classical single-track model which is obtained by lumping the two front wheels as one wheel in the centerline of the vehicle (the same is done with the two rear wheels) [3]. For the lateral direction and the yaw axis, the vehicle kinetics at the CG are described as

$$ma_y = 2\left(F_f + F_r\right) \quad \text{and} \tag{1}$$

$$I_{zz}\,\dot{\gamma} = 2a\left(F_f - F_r\right) \tag{2}$$

where $a_y$, $\gamma$, $m$, $I_{zz}$, $F_f$ and $F_r$ are lateral acceleration, the yaw rate, the total vehicle mass, the yaw moment of inertia, the lateral force at the front tire, and the lateral force at the rear tire, respectively, and $a$ is the distance from the vehicle CG to the front axle. Because tires can be modeled as linear within $|a_y| \le 0.3g$, the lateral forces at the front and rear tires are obtained as

$$F_f = C_f \cdot \alpha_f \quad \text{and} \tag{3}$$

$$F_r = C_r \cdot \alpha_r \tag{4}$$

where $C_f$ and $C_r$ are the front and rear cornering stiffnesses respectively. The front and rear side slip angles, $\alpha_f$ and $\alpha_r$, respectively, are approximately expressed as

$$\alpha_f = \delta - \frac{a \cdot \gamma + v}{u} \quad \text{and} \tag{5}$$

$$\alpha_r = \frac{b \cdot \gamma - v}{u} \tag{6}$$

where $\delta$ is the steering angle, $u$ and $v$ are the lateral and the longitudinal velocities of the vehicle at CG, respectively, and $b$ is the distance from the vehicle CG to the rear axle. By the vehicle kinematics, $a_y$ at CG is given by

$$a_y = \dot{v} + u \cdot \gamma. \tag{7}$$

### *2.2 Multi body dynamic vehicle model*

To improve the accuracy of a vehicle model in simulation, bushing is considered between suspension systems and chassis [3]. A bushing made of rubber is modeled as each three-dimensional translational spring damper actuator (TSDA) and rotational spring damper actuator (RSDA). In total, there are six stiffness parameters and six damping parameters. The left and right front suspensions are separated; they are of the double wishbone type in which shock absorbers are modeled as TSDAs. To reduce vehicle rolling, a stabilizer bar is considered. The rear left and right suspensions are of the four link type. Fig. 1 presents the front and rear suspension systems where R, S, T, U, and B denote the revolution joint, spherical joint, translational joint, universal joint, and bushing, respectively. The body parts are tire ①/⑨, front right knuckle ②, front upper/lower arm ③/④, front tie rod ⑤, rack & pinion ⑥, front shock absorber ⑦/⑩, front torsion bar ⑧, rear spring ⑩, lower/upper arm link ⑫/⑬, and rear axle ⑭. Because the tire is the only mediator transferring the actuating, breaking, and steering forces between the vehicle and the road, it is the most important component in the field of vehicle dynamics. In this paper, tires are modeled theoretically, assuming a point contact on the road.

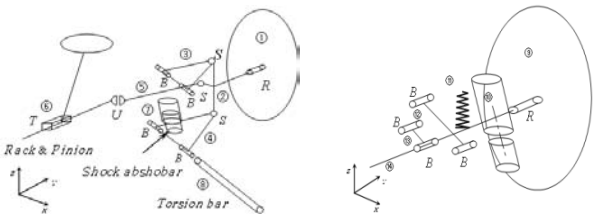


(a) Double wishbone-type front right suspension (b) Four-links-type rear suspension

Fig. 1. Full vehicle model by multi body dynamics.

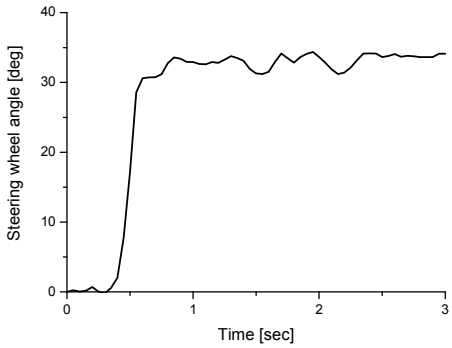


Fig. 2. Steering wheel angle input for model verification.

### *2.3 Model verification*

To verify the modeled vehicle, its dynamic characteristics are compared with those of an actual vehicle. In general, the J-turn test is carried out to verify the handling performance such as the rollover or riding performance. In the simulation, the steering wheel angle is increased to 34° within 0.2s as shown in Fig. 2, where the longitudinal velocity is 22 m/s. Fig. 3 presents the results of the J-turn for the single-track model, the multi body model, and the actual vehicle. Their yaw rates are larger than 8°/s as illustrated in Fig. 2(a). The single-track model and the multi body model have characteristics that are similar to those of the actual vehicle.

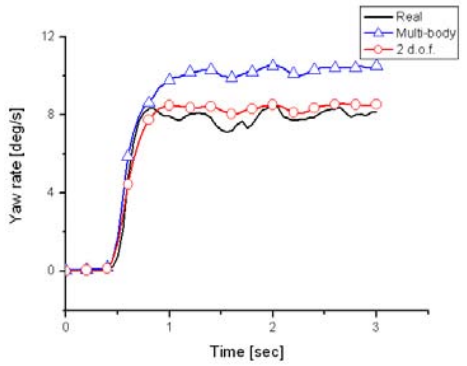


(a) Yawrate

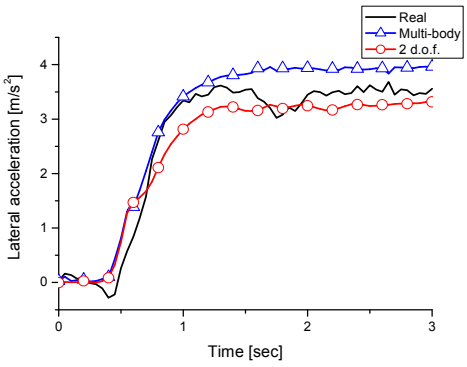


(b) Lateral acceleration

Fig. 3. Model verification results.

## 3. Lateral controller of an autonomous vehicle

### *3.1 LMI based H∞ control [13]*

The H∞ norm of a stable transfer function $G(s)$ is its largest input/output root mean square (rms) gain, i.e.,

$$\|G(s)\| = \sup \frac{\|\mathrm{y}(t)\|_{L_2}}{\|\mathrm{u}(t)\|_{L_2}} \tag{8}$$

where $L_2$ is the space of signals with finite energy and $\mathrm{y}(t)$ is the output of the system $G(s)$ for a given input $\mathrm{u}(t)$. In its abstract standard formulation, the H∞ control problem is one of disturbance rejection. This can be interpreted as minimizing the effect of the worst-case disturbance $w$ on the output $z$. The LMI-based approach has the advantage of eliminating the regularity restrictions attached to the Riccati-based solution. The system is given in state-space form by

$$\dot{x} = Ax + B_1 w + B_2 \mathrm{u}, \tag{9}$$

$$z = C_1 x + D_{11} w + D_{12} \mathrm{u}, \quad \text{and} \tag{10}$$

$$y = C_2 x + D_{21} w + D_{22} \mathrm{u}. \tag{11}$$

The Riccati-based approach is applicable to plants $P$ satisfying $D_{12}$ and $D_{21}$ have full rank, transfer functions from control input $u(s)$ to state $z(s)$ and from disturbance $w(s)$ to output $y(s)$ have no zeros on the $j\omega$-axis. Given $\gamma > 0$, it gives necessary and sufficient conditions for the existence of internally stabilizing controllers $K(s)$ such that $\|F(P,K)\|_\infty < \gamma$.

Specifically, the H∞ performance $\gamma$ is achievable if and only if there are 6 constraint equations. Then the optimal H∞ performance $\gamma_{\mathrm{opt}}$ can be computed by $\gamma$ –iterations. In comparison, the H∞ performance is directly optimized by solving the following LMI problem:

$$\begin{bmatrix} N_{21} & 0 \\ 0 & I \end{bmatrix} \begin{bmatrix} AR + RA^T & RC_1^T & B_1 \\ C_1 R & -\gamma I & D_{11} \\ B_1^T & D_{11}^T & -\gamma I \end{bmatrix} \begin{bmatrix} N_{12} & 0 \\ 0 & I \end{bmatrix} < 0, \tag{12}$$

$$\begin{bmatrix} N_{12} & 0 \\ 0 & I \end{bmatrix} \begin{bmatrix} A^T S + SA & SB_1 & C_1^T \\ B_1^T R & -\gamma I & D_{11}^T \\ C_1 & D_{11} & -\gamma I \end{bmatrix} \begin{bmatrix} N_{21} & 0 \\ 0 & I \end{bmatrix} < 0, \quad \text{and} \tag{13}$$

$$\begin{bmatrix} R & I \\ I & S \end{bmatrix} \geq 0 \tag{14}$$

where $N_{12}$, $N_{21}$ denote bases of the null spaces of $\left(B_2^T, D_{12}^T\right)$, $\left(C_2, D_{21}\right)$ and $R, S$ are real coefficient matrices.

The selection of weighting functions for a specific design problem often involves ad hoc fixing, much iteration, and fine tuning. It is very difficult to provide a general formula for weighting functions that will work in every case. Based on time domain performance specifications, the corresponding requirements in the frequency domain; in terms of the bandwidth $w_b$, the peak sensitivity $M_S$, and the steady-state margin $\varepsilon$ can be determined. A possible choice of error weighting function $W_e$ can be obtained by modifying the weighting function as follows [14]:

$$W_e = \frac{s/M_s + w_b}{s + w_b \varepsilon}. \tag{15}$$

The magnitude $|K(s)S(s)|$ of controller $K(s)$ times the sensitivity function $S(s)$ in the low-frequency range is essentially limited by the allowable cost of control effort and the saturation limit of the actuators. Hence, in general, the maximum gain $M_u$ of $|K(s)S(s)|$ can be fairly large, whereas the high-frequency gain is essentially limited by the controller bandwidth $w_{bc}$ and the sensor noise frequencies margin $\varepsilon_1$. A candidate input weight function $W_u$ would be

$$W_u = \frac{s + w_{bc}/M_u}{\varepsilon_1 s + w_{bc}}. \tag{16}$$

The weighting for MIMO problems can initially be chosen as diagonal matrices, with each diagonal term chosen as above.

So the controller design procedure is as follows:

(1) Derive a generalized plane,
(2) Select weighting functions,
(3) Find $\gamma$ to satisfy Eqs. (12)-(14).

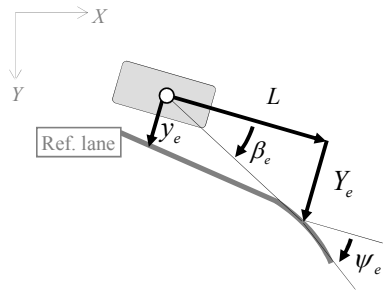


Fig. 4. Sensing information for lateral control.

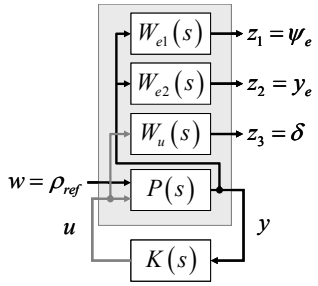


Fig. 5. Generalized plant for lateral control by target yaw angle and lateral offset.

### *3.2 Look-ahead sensing method*

In previous research [2, 11], the headings at the origin and the target point were assumed to be tangential angles of a curve going through the origin and the target point $(L, Y_e)$, as illustrated in Fig. 4. Then, the cubic curve that goes through the two points, as shown in Fig. 4, is uniquely defined as follows:

$$y = A_t x^3 + B_t x^2 \tag{17}$$

where $A_t = \dfrac{L \cdot \tan\psi_e - 2Y_e}{L^3}$ and $B_t = \dfrac{3Y_e - L \cdot \tan\psi_e}{L^2}$.

Because the desired trajectories to the target point are independent of the longitudinal velocity $u$ in the non slip vehicle model, the steering control angle $\delta$ that leads the vehicle to hit the target point $(L, Y_e)$ with the heading $\psi_e$ is given as follows:

$$\delta = \tan^{-1}(2lB_t) \tag{18}$$

where $l$ is the wheelbase of a vehicle. However, the information of the lane is satisfied with

$$Y_e(3Y_e - L \cdot \tan\psi_e) < 0\,. \tag{19}$$

Therefore, it may be impossible to track the reference lane if the speed of vehicle is high. To the lateral control using this cubic curve method should be modified for high-speed maneuvering.

In the research by Kim [15], the basic algorithm for the lateral control is to minimize the target heading angle error $\beta_e$ at the look-ahead point. Kim [13] introduced the H$\infty$ controller where the state vector $X_0 = [v \quad \gamma \quad \beta_e]^T$ and the output vector $Y_0 = \beta_e$.

### *3.3 Proposed lateral control algorithm*

The previous lateral control algorithm by target heading angle is the correct method for coping with the change of lane curvature. However, the lateral offset $y_e$ as tracking performance is disregarded. In order to reduce the lateral offset and improve handling performance at the same time, the controller is designed to minimize the error of the lateral offset at the CG and the error of the target yaw angle at the look-ahead point. Through the fusion of look-down sensing by the MR or MPC sensor and look-ahead vision or virtual sensing by GPS, this modified control algorithm can be implemented. Here, the errors are also minimized by the LMI-based H$\infty$ control algorithm. Through the combination of the 2 DOF vehicle dynamics and the lane geometry, the state space model for the state vector $X_0 = [v \quad \gamma \quad \psi_e \quad y_e]^T$ and the output vector $Y_0 = [\psi_e \quad y_e]$ is written as

$$\dot{X}_0 = A_0 X_0 + B_{01}\rho_{ref} + B_{02}\delta \quad \text{and} \quad Y_0 = C_0 X_0 \tag{20}$$

where $\rho_{ref}$ is the curvature of a reference lane as disturbance and system matrices are calculated by

$$A_0 = \begin{bmatrix} -\dfrac{2(C_f + C_r)}{mu} & -u - \dfrac{2(aC_f - bC_r)}{mu} & 0 & 0 \\ -\dfrac{2(aC_f - bC_r)}{I_{zz}u} & -\dfrac{2(a^2C_f + b^2C_r)}{I_{zz}u} & 0 & 0 \\ 0 & -1 & 0 & 0 \\ -1 & -L & u & 0 \end{bmatrix},$$

$$B_{01} = \begin{bmatrix} \dfrac{2C_f}{m} \\ \dfrac{2aC_f}{I_{zz}} \\ 0 \\ 0 \end{bmatrix}, B_{02} = \begin{bmatrix} 0 \\ 0 \\ u \\ 0 \end{bmatrix}, \text{ and } C_0 = \begin{bmatrix} 0 & 0 & 1 & 0 \\ 0 & 0 & 0 & 1 \end{bmatrix}. \tag{21}$$

The control objectives, $z_1$, $z_2$, and $z_3$ represent the target yaw angle error $\psi_e$, the lateral offset $y_e$, and the steering control input $\delta$. The generalized plant, as illustrated in Fig. 5, can be represented as the state space model.

$$\dot{X} = \begin{bmatrix} A_{e1} & 0 & 0 & B_{e1}\begin{bmatrix}1 & 0\end{bmatrix}C_0 \\ 0 & A_{e2} & 0 & B_{e2}\begin{bmatrix}0 & 1\end{bmatrix}C_0 \\ 0 & 0 & A_u & 0 \\ 0 & 0 & 0 & A_0 \end{bmatrix} X + \begin{bmatrix} 0 \\ 0 \\ 0 \\ B_{01} \end{bmatrix} \rho_{ref} + \begin{bmatrix} 0 \\ 0 \\ B_u \\ B_{02} \end{bmatrix} \delta$$

$$Z = \begin{bmatrix} C_{e1} & 0 & 0 & D_{e1}C \\ 0 & C_{e2} & 0 & D_{e2}C_0 \\ 0 & 0 & C_u & 0 \end{bmatrix} X + \begin{bmatrix} 0 \\ 0 \\ 0 \end{bmatrix} \rho_{ref} + \begin{bmatrix} 0 \\ 0 \\ D_u \end{bmatrix} \delta \tag{22}$$

$$Y = \left[\begin{array}{ccc|c} 0 & 0 & 0 & C_0 \\ 0 & 0 & 0 & \end{array}\right] X + \begin{bmatrix} 0 \\ 0 \end{bmatrix} \rho_{ref} + \begin{bmatrix} 0 \\ 0 \end{bmatrix} \delta$$

For the generalized plant, the controller is designed to satisfy Eqs. (12)-(14).

## 4. Simulation results

### *4.1 Weighting functions for $H_\infty$ controllers*

In the target heading method and the proposed lateral offset and target yaw angle method, the control input weighting function is tuned by

$$W_u = \frac{s + 0.008727}{0.001s + 0.008727}. \tag{23}$$

The error weighting functions for each controller are tuned by

$$W_{\beta_e} = \frac{s + 100}{s + 0.001},\ W_{\psi_e} = \frac{0.1s + 50}{s + 0.001},\ \text{and}\ W_{y_e} = \frac{10s + 0.1}{s + 0.001}. \tag{24}$$

Fig. 6 shows the bode plots from the curvature of a reference to the look-down lateral offset and the look-ahead target yaw angle error.

### *4.2 Results for the nominal model*

In this study, an autonomous vehicle is controlled to change a lateral 3.5 m straight lane and to track a circular lane of radius 300 m at a constant longitudinal velocity of 22 m/s (approximately 80 km/h). In the proposed lateral control, the steering input $\delta$ is larger than in the previous controller and the vehicle rapidly change reference lanes, as illustrated in Fig. 7. Generally, a lateral controller should balance tracking performance (settling time $t_s$, lateral overshoot) and handling performance (yaw rate, lateral acceleration). In the lane tracking, the proposed controller has the smallest lateral offset $y_e$, as illustrated in Fig. 8. The abrupt change of curvatures on the road introduces sudden changes into the control loop and results in poor ride comfort to car passengers. The simulation results for lane change and tracking are summarized in Tables 1 and 2.

### *4.3 Robustness of the lateral control*

The robustness against the perturbation of vehicle mass, cornering stiffness, and sensing noises are analyzed in the circular lane tracking. As the mass of a vehicle is increased, the vehicle dynamics become slower so that the lateral offsets by the robust controllers are decreased. In the cubic curve method, the steering input is increased but the lateral offset is also increased. The cornering stiffness of a vehicle is influenced by tire and road conditions. With increasing stiffness, the steering inputs are decreased and lateral offsets are increased, as summarized in Table 3. Generally, the pattern of

Table 1. Simulation results for lane change (3.5m).

| | | Cubic curve | Heading angle | Proposed |
|---|---|---|---|---|
| Tracking | $\delta$ max [deg] | 1.2061 | 0.6537 | 4.3662 |
| | $t_s$ [sec] | 2.60 | 2.92 | 1.29 |
| | $y_e$ max [m] | 1.1027 | 1.1608 | 0.8656 |
| Handling | $\gamma$ max [deg/s] | 6.8154 | 4.4668 | 24.2618 |
| | $a_y$ max [m/s$^2$] | 1.9692 | 1.5093 | 6.0172 |

Table 2. Simulation results for circular lane tracking (radius: 300m).

| | | Cubic curve | Heading angle | Proposed |
|---|---|---|---|---|
| Tracking | $\delta$ max [deg] | 0.6668 | 0.7643 | 0.8714 |
| | $y_e$ max [m] | 0.6406 | 0.2966 | 0.1744 |
| Handling | $\gamma$ max [deg/s] | 4.5621 | 5.2471 | 5.6725 |
| | $a_y$ max [m/s$^2$] | 1.7483 | 1.9734 | 1.8548 |

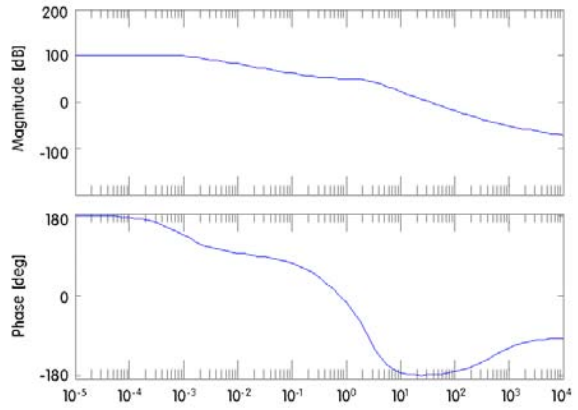


(a) Look-down lateral offset

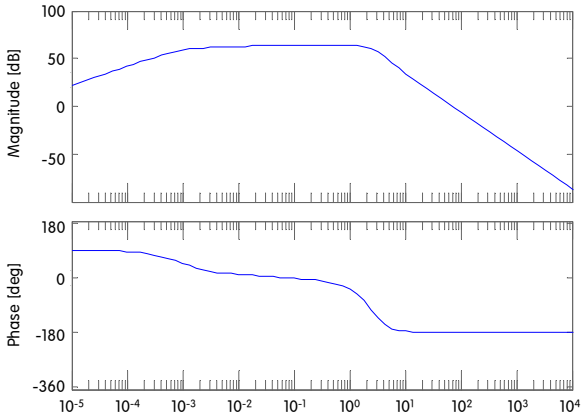


(b) Look-ahead target yaw angle

Fig. 6. The bode plots of the closed-loop system.

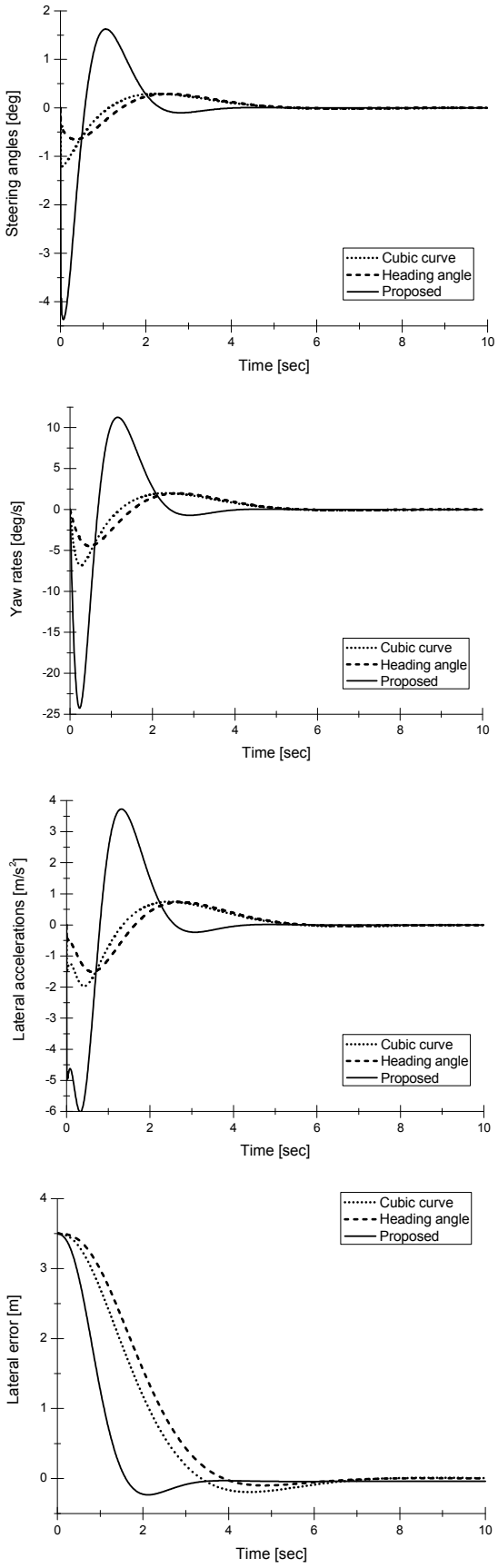


Fig. 7. Simulation results in straight lane change.

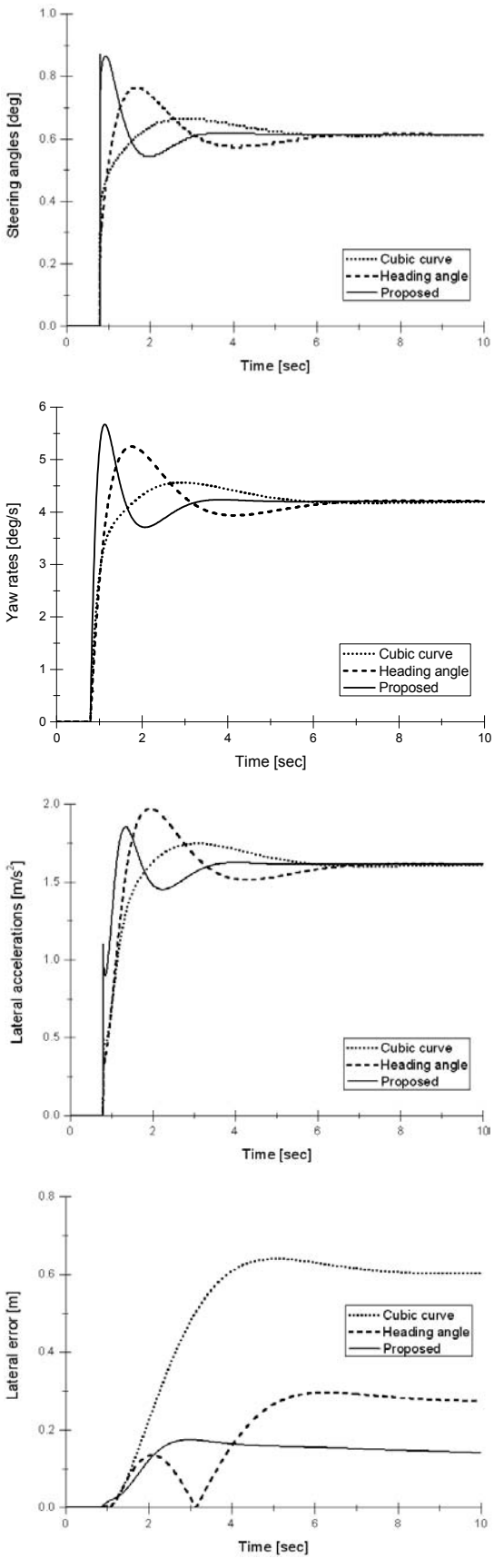


Fig. 8. Simulation results in circular lane tracking.

Table 3. Robustness against modeling uncertainties.

| | | Cubic curve | | Heading angle | | Proposed | |
|---|---|---|---|---|---|---|---|
| | | $\delta$ STD [deg] | $y_e$ mean [m] | $\delta$ STD [deg] | $y_e$ mean [m] | $\delta$ STD [deg] | $y_e$ mean [m] |
| Mass | *Nominal* | 0.0150 | 0.5859 | 0.0238 | 0.2332 | 0.0210 | 0.1027 |
| | +100kg | 0.0161 | 0.6294 | 0.0236 | 0.1819 | 0.0203 | 0.0894 |
| | +200kg | 0.0172 | 0.6729 | 0.0233 | 0.1312 | 0.0196 | 0.0761 |
| | +300kg | 0.0183 | 0.7164 | 0.0231 | 0.0814 | 0.0189 | 0.0629 |
| | +400kg | 0.0194 | 0.7598 | 0.0230 | 0.0366 | 0.0182 | 0.0496 |
| | +500kg | 0.0205 | 0.8033 | 0.0229 | 0.0458 | 0.0176 | 0.0364 |
| Cornering stiffness | -20% | 0.0191 | 0.7664 | 0.0259 | 0.0357 | 0.0230 | 0.0478 |
| | -10% | 0.0167 | 0.6662 | 0.0247 | 0.1402 | 0.0219 | 0.0783 |
| | *Nominal* | 0.0150 | 0.5859 | 0.0238 | 0.2332 | 0.0210 | 0.1027 |
| | +10% | 0.0137 | 0.5203 | 0.0231 | 0.3108 | 0.0204 | 0.1226 |
| | +20% | 0.0127 | 0.4656 | 0.0225 | 0.3764 | 0.0198 | 0.1393 |

Table 4. Robustness against random sensing noises.

| | | Cubic curve | | Heading angle | | Proposed | |
|---|---|---|---|---|---|---|---|
| | | $\delta$ STD [deg] | $y_e$ mean [m] | $\delta$ STD [deg] | $y_e$ mean [m] | $\delta$ STD [deg] | $y_e$ mean [m] |
| Position | *Nominal* | 0.0150 | 0.5859 | 0.0238 | 0.2332 | 0.0210 | 0.1027 |
| | ±0.01m | 0.0151 | 0.5861 | 0.0238 | 0.2331 | 0.0220 | 0.1026 |
| | ±0.02m | 0.0156 | 0.5860 | 0.0239 | 0.2331 | 0.0249 | 0.1027 |
| Yaw angle | *Nominal* | 0.0150 | 0.5859 | 0.0238 | 0.2332 | 0.0210 | 0.1027 |
| | ±1deg | 0.1199 | 0.5867 | 0.0574 | 0.2327 | 0.3139 | 0.1024 |
| | ±2deg | 0.2383 | 0.5856 | 0.1053 | 0.2372 | 0.6255 | 0.1032 |

sensing noise depends on the sensor system. In this paper, uniformly distributed random noises are added in vehicle position (maximum ±0.01, 0.02 m) and yaw angle (maximum ±1, 2°). Table 4 summarizes the simulation results related to sensing noises and reveals that all of the controllers are robust against the sensing noises. Figs. 9 and 10 illustrate the lane change and tracking results with an additional mass of 500 kg, 20% increased cornering stiffness, and sensing noises in position (±0.01 m) and yaw angle (±2 °).

## 5. Conclusions

This paper examined the lateral control of an autonomous vehicle. A robust LMI-based $H_\infty$ controllers that utilized the feedback of the (look-ahead) target yaw angle and the (look-down) lateral offset was proposed against the high-frequency sensor noises and the modeling uncertainties. This controller minimizes the effect of the curvature of a reference lane on the target yaw angle error, the lateral offset, and the steering control input by solving the LMI problem. In the implementation of lateral control, a look-ahead method generally utilizes a vision system. For a look-down method, GPS, MR, or MPC sensors are employed. The proposed lateral control algorithm is effective for the sensor fusion of look-ahead and look-down. In the simulations of multi body dynamics, the lateral offset

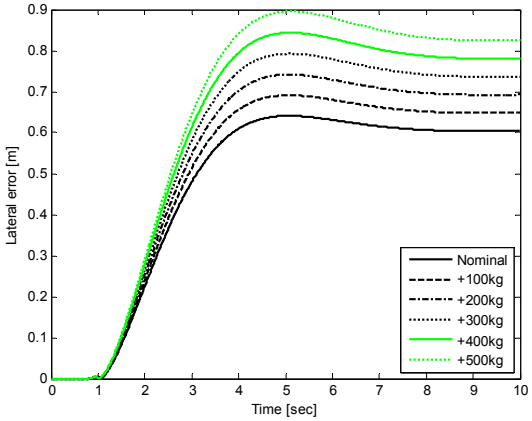


(a) Cubic curve method

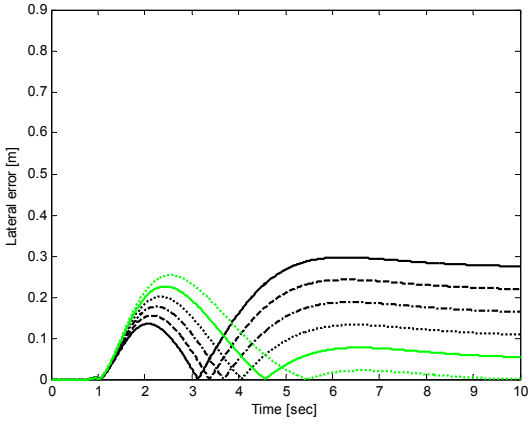


(b) Heading angle method

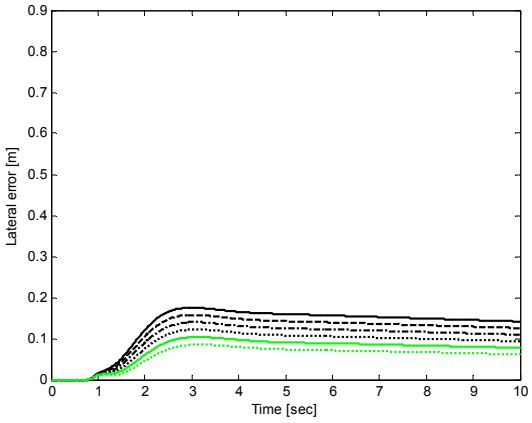


(c) Proposed method

Fig. 9. Simulation results for mass addition.

by the proposed algorithm is smaller than that in other look-ahead controllers despite the sensing noises and the perturbation in mass and cornering stiffness. In actual vehicles, lateral controllers should balance handling and tracking performances by expert drivers.

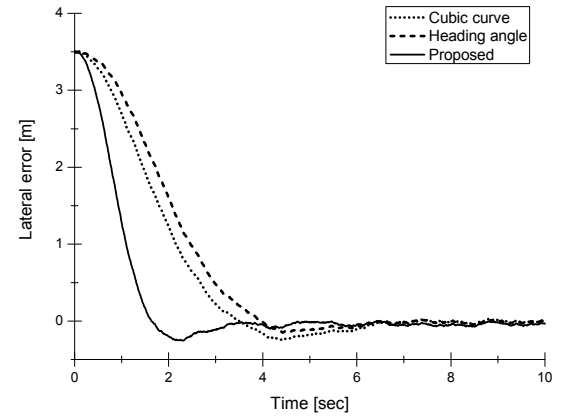


(a) Lane change

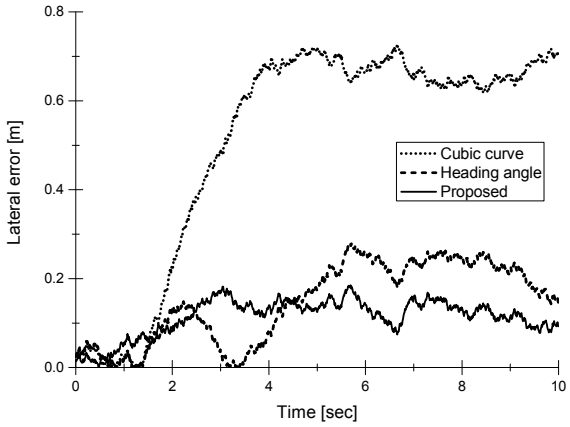


(b) Circular lane tracking

Fig. 10. Simulation results for modeling uncertainties and sensing noises.

## Acknowledgment

This research was supported by Kyungsung University Research Grants in 2011.

## References

[1] H. S. Tan, J. Guldner, S. Patwardhan, C. Chen and B. Bougler, Development of an automated steering vehicle based on roadway magnets-a case study of mechatronic system design, *IEEE/ASME Transactions on Mechatronics*, 4 (3) (1999) 258-272.

[2] S. Tsugawa, Vision-based vehicles in Japan: machine vision systems and driving control systems, *IEEE Transactions on Industrial Electronics*, 41 (4) (1994) 389-405.

[3] J. Y. Choi, S. J. Hong, K. T. Park, W. S. Yoo and M. H. Lee, Lateral control of autonomous vehicle by yaw rate feedback, *Journal of Mechanical Science and Technology*, 16 (3) (2002) 338-343.

[4] E. J. Rossetter, J. P. Switkes and J. C. Gerdes, Experimental validation of the potential field lanekeeping system, *International Journal of Automotive Technology*, 5 (2) (2004) 95-108.

[5] J. Ackermann, J. Guldner, W. Sienel, R. Steinhauser and V. I. Utkin, Linear and nonlinear controller design for robust automatic steering, *IEEE Transactions on Control Systems Technology*, 3 (1) (1995) 132-143.

[6] Fritz, Longitudinal and lateral control of heavy duty trucks for automated vehicle following in mixed traffic: experimental results from the CHAUFFEUR project, *Proceeding of the IEEE International Conference of Control Application, Hawai'i, USA* (1999) 1348-1352.

[7] H. Makela and T. V. Numers, Development of a navigation and control system for an autonomous outdoor vehicle in a steel plant, *Control Engineering Practice,* 9 (2001) 573-583.

[8] R. Rajamani, H. S. Tan, B. K. Law, and W. B. Z, Demonstration of integrated longitudinal and lateral control for the operation of automated vehicles in platoons, *IEEE Transactions on Control Systems Technology*, 8 (8) (2000) 695-707.

[9] K. B. Lee, Y. J. Kim, O. S. Ahn and Y. B. Kim, Lateral control of autonomous vehicle using Levenberg-Marquardt neural network algorithm, *International Journal of Automotive Technology*, 3 (2) (2002) 71-77.

[10] M. M. Chen, T. Jochem, and D. Pomerleau, AURORA: a vision-based roadway departure warning system, *Proceedings of the 1995 IEEE/RSJ International Conference on Intelligent Robots and Systems*, 1 (1995) 243-248.

[11] S. Tsugawa, An overview on control algorithms for automated highway systems, *IEEE/IEEJ/JSAI International Conference* (1999) 234-239.

[12] J. M. Lee, Unmanned navigation of vehicle using the ultrasonic positioning system, *Master's thesis, Pusan National University, Korea, Department of Interdisciplinary Program in Mechatronics Graduate School* (2004).

[13] P. Gahinet, A. Nemirovski, A. J. Laub and M. Chilali, *LMI Control Toolbox for User with MATLAB*, The MathWorks, Inc. (1995).

[14] K. Zhou and J. C. Doyle, *Essentials of Robust Control*, Prentice-Hall International (1998) 81-102.

[15] C. S. Kim, S. Y. Kim, J. H. Ryu and M. H. Lee, LMI-based $H_\infty$ lateral control of an autonomous vehicle by look-ahead sensing, *International Journal of Automotive Technology*, 7 (5) (2006) 609-618.

**Ju Yong Choi** received his B.S., M.S., and Ph.D degrees in 1998, 2000, and 2005 from the Pusan National University, Korea. From 2005 to 2009, he worked in Hyundai-Kia R&D Center and he was a senior researcher at the automotive parts innovation center from 2009 to 2011. He is currently a professor at Kyungsung University. His research interests are in the area of autonomous vehicle, chassis control system and hardware-in-the-loop simulation system.